Am J Cancer Res 2023;13(10):4888-4902
www.ajcr.us /ISSN:2156-6976/ajcr0148926

Original Article

Small-molecule exhibits anti-tumor activity by targeting the RNA m^{6}A reader IGF2BP3 in ovarian cancer

Chang Shu[1,2*], Mao-Hong Gu[3*], Cheng Zeng[4], Wen-Gui Shao[1], Hai-Yang Li[4], Xin-Hua Ma[1], Mu-Xing Li[1], Yuan-Yuan Cao[4], Meng-Jie Zhang[1], Wei Zhao[5], Shu-Li Zhao[1,4]

[1]*General Clinical Research Center, Nanjing First Hospital, China Pharmaceutical University, Nanjing, Jiangsu, China;* [2]*Department of Pharmacy, Affiliated Hospital of Yangzhou University, Yangzhou, Jiangsu, China;* [3]*Department of Obstetrics and Gynecology, Nanjing First Hospital, Nanjing Medical University, Nanjing, Jiangsu, China;* [4]*General Clinical Research Center, Nanjing First Hospital, Nanjing Medical University, Nanjing, Jiangsu, China;* [5]*Department of Pathology, Nanjing First Hospital, Nanjing Medical University, Nanjing, Jiangsu, China.* [*]*Equal contributors.*

Received January 3, 2023; Accepted September 6, 2023; Epub October 15, 2023; Published October 30, 2023

Abstract: Based on its absence in normal tissues and its role in tumorigenesis and tumor progression, insulin-like growth factor 2 mRNA-binding protein 3 (IGF2BP3), a reader of N6-methyladenosine (M^{6}A) on RNA, represents a putative valuable and specific target for some cancer therapy. In this study, we performed bioinformatic analysis and immunohistochemistry (IHC) to find that IGF2BP3 was highly expressed in tumor epithelial cells and fibroblasts of ovarian cancer (OC), and was associated with poor prognosis, metastasis, and chemosensitivity in OC patients. In particular, we discovered that knockdown IGF2BP3 expression inhibited the malignant phenotype of OC cell lines by decreasing the protein levels of c-MYC, VEGF, CDK2, CDK6, and STAT1. To explore the feasibility of IGF2BP3 as a therapeutic target for OC, a small molecular AE-848 was designed and screened by molecular operating environment (MOE), which not only could duplicate the above results of knockdown assay but also reduced the expression of c-MYC in M2 macrophages and tumor-associated macrophages and promoted the cytokine IFN-γ and TNF-α secretion. The pharmacodynamic models of two kinds of OC bearing animals were suggested that systemic therapy with AE-848 significantly inhibited tumor growth by reducing the expression of tumor-associated antigen (c-MYC/VEGF/Ki67/CDK2) and improving the anti-tumor effect of macrophages. These results suggest that AE-848 can inhibit the growth and progression of OC cells by disrupting the stability of the targeted mRNAs of IGF2BP3 and may be a targeted drug for OC treatment.

Keywords: IGF2BP3, ovarian cancer, inhibitors, RNA m^{6}A, targeted agents

Introduction

Ovarian cancer (OC) has become the deadliest gynecologic tumor, with more than 220,000 women diagnosed each year worldwide [1]. Due to the lack of early symptoms, about three-quarters of OC patients have an advanced stage at the first diagnosis [2]. Despite advances in surgery, chemotherapy, and new immunotherapies, overall survival (OS) of all stages of OC remains poor [3, 4]. There is an urgent need to find new and effective therapeutic targets and therapeutic drugs to improve the situation.

Recently, an increasing number of novel m^{6}A regulatory enzymes have been identified. Insulin-like growth factor 2 mRNA binding proteins (IGF2BPs) are a new family of m^{6}A readers, which consists of three RNA-binding proteins, including IGF2BP1, IGF2BP2, and IGF2BP3 [5]. IGF2BPs has been reported to preferentially recognize m^{6}A-modified mRNAs and promote mRNA stability of numerous target genes in a m^{6}A-dependent manner, thereby enhancing the expression of target genes [6, 7]. In addition, IGF2BPs could enhance mRNA storage or inhibit mRNA degradation under stress conditions, thus promote translation. Studies have confirmed that IGF2BP3 predicted disease progression and prognosis in patients with ovarian clear cell carcinoma, and overexpression of IGF2BP3 promoted the invasion of ovarian clear cell cancer cells [8, 9]. However,

the role of IGF2BP3 in m^{6}A reading in OC remains unclear.

Small molecule inhibitors are a class of small molecule compounds that can bind and reduce the biological activity of target proteins, and have significant advantages in the fine regulation of cell life and function [10]. At present, using high-throughput virtual screening methods, drug molecules with novel structures can be quickly screened from the database, so as to improve the success rate of new drug development, reduce costs, and shorten the development cycle.

This study aims to screen out a small molecule inhibitor targeting IGF2BP3, which is highly expressed in OC, by using small molecule docking technology. *In vitro* and *in vivo* experiments were conducted to analyze the inhibitory effect of this small molecule inhibitor on OC cells and its mechanism.

Materials and methods

Bioinformatics analysis of clinical data

Analysis of m^{6}A read proteins in OC was performed using the Gene Expression Profiling Interactive Analysis (GEPIA) database (http://gepia.cancer-pku.cn/). Raw gene expression data for ovarian cancer were retrieved from the Cancer Genome Atlas (TCGA) and Genotype-Tissue Expression (GETx) which were downloaded through the University of California Santa Cruz Xena (UCSC Xena, https://xena.ucsc.edu/). The Kaplan-Meier Plotter online analysis tool (https://kmplot.com/analysis/) was used to perform Kaplan-Meier analyses of patients with ovarian cancer from the Xena database.

Immunohistochemical (IHC) staining

Paraffin-embedded sections were subjected to IHC examination. Sections were dewaxed in xylene (I, II, II), reduced ethanol concentration (100, 95, 80, 75%), hydrated for 5 min each time, and microwave heated in sodium citrate buffer to repair antigens. Then, sections were closed with 5% bovine serum albumin and incubated with anti-rabbit polyclonal antibodies overnight at 4°C. Next, the sections were treated with horseradish peroxidase (HRP)-labeled rabbit secondary antibody. Then incubate with a DAB substrate kit to develop the color. After washing in PBS, the tissue sections were re-stained with hematoxylin and observed under an orthomosaic microscope. The primary antibodies used in the study included anti-IGF2BP3 antibody (1:200; OAAN01146, AVIVA SYSTEMS BIOLOGY), anti-CDK2 antibody (1:200; 10122-1-AP, Proteintech), anti-VEGF antibody (1:200; 19003-1-AP, Proteintech), anti-KI67 antibody (1:1000; ab279653; Abcam) and anti-c-MYC antibody (1:500; 67447-1-Ig, Proteintech).

Cell culture and cell transfection

The human OC cell lines A2780 and HO8910, human monocyte cell line THP-1, and mouse OC cell line ID8 were purchased from the Type Culture Center, Chinese Academy of Sciences (Shanghai, China). A2780, HO8910, and ID8 were cultured in DMEM. THP-1 cells were cultured in a RPMI-1640 culture medium (KeyGEN Biotech). All media contained 1% penicillin/streptomycin and 10% fetal bovine serum (FBS, Gibco). Cells were cultured in humid air at 37°C, with 5% CO_2.

The human IGF2BP3 gene was amplified by qRT-PCR and cloned into a pcDNA vector plasmid to generate an IGF2BP3 overexpression plasmid (pcDNA-IGF2BP3), and an empty vector plasmid (pcDNA-NC) was used as a negative control. The small interfering RNA (siRNA) used for cell transfection of IGF2BP3 was designed and synthesized by Hanbio (Shanghai, China). According to the manufacturer's instructions, the siRNA was transfected into human ovarian cancer cells with Lipofectamine 2000 (Invitrogen, USA). Cells after 72 hours of transfection were screened with puromycin (2 μg/mL) for one week, and IGF2BP3 expression was detected by real-time quantitative qRT-PCR and Western blotting.

Quantitative real-time polymerase chain reaction (qRT-PCR)

Total RNA was extracted with TRIzol reagent (Invitrogen) according to the manufacturer's protocol, dissolved in RNA-free ddH_2O, and stored at -80°C. cDNA synthesis was performed from each 1 μg RNA sample using a reverse transcriptase kit (Vazyme). Then, qPCR was performed using the SYBR Green PCR kit (Vazyme) on a real-time detector (Q5). expression data were calculated using the $2^{-\Delta\Delta Ct}$ method and normalized using GAPDH as an internal

reference to control relative expression levels. The primers for RT-qPCR were shown in Supplementary Table 1.

Western blotting

Proteins were extracted from cells using RIPA buffer (KeyGene Biotech) with protease inhibitor cocktail and phosphatase inhibitor cocktail (KeyGene Biotech), and protein concentrations were measured using the BCA protein assay kit (KeyGene Biotech). Total protein samples were separated by 10% or 15% sodium dodecyl sulfate-polyacrylamide gel electrophoresis (SDS-PAGE) and transferred to PVDF membranes (Millipore, USA). The membranes were rinsed with 1×TBST, blocked with 5% skim milk in 1×TBST for 3 h at room temperature, and then incubated with different primary antibodies overnight at 4°C, the membranes were washed three times with 1×TBST, and the membranes were incubated with HRP-coupled goat anti-rabbit secondary antibodies for 2 h at room temperature. The membranes were then rinsed five times with 1×TBST for 7 min each. Using ECL detection reagents, the signals were visualized on a chemiluminescence instrument (New Cell and Molecular Biotech, Suzhou, China). The integrated relative density of individual bands was quantified using Image J.

Cell proliferation

Cell proliferation was tested using the Cell Counting Kit-8 (APExBIO). Each well of a 96-well culture plate was seeded with approximately 5×10^3 target cells and maintained at 37°C overnight. At 0, 12, 24, 48, 60, and 72 hours after transfection, cells were treated with CCK-8 (10 μL/well) and incubated for 2 hours. Subsequently, the optical density of each well was read at 450 nm. Every sample was assayed three times.

Cell cycle assay

For cell cycle assay, 1×10^6 cells were harvested, fixed in 70% ethanol, and stored at 4°C overnight. Cells were then stained with PI staining solution for 30 min in the dark at room temperature followed by flow cytometry. The fractions of the cells in the G1, S, and G2/ phases were calculated with Modfit software (Verity Software House, USA).

Transwell invasion assay

Transwell invasion assays were performed using Transwell chambers (Costar Corporation, USA) with Matrigel (Corning, USA). For invasion assays, Transwell chambers were coated with Matrigel (1:8 dilution; Corning, USA) and left at 37°C for 12 hours. 5×10^4 cells were resuspended in 200 μL serum-free medium and seeded into the upper chamber. Then 700 μL of 10% FBS medium was then added to the lower chamber. After incubation at 37°C for 48 h, cells were fixed with 4% formaldehyde for 30 min, and then adherent cells were removed and rinsed once with PBS. The cells were stained with 1 ml/well of 0.5% crystal violet for 30 min and washed three times with PBS. Finally, the number of cells on the luminal floor was counted by magnifying microscopy.

Wound healing assay

Cells (10^6 cells/well) are inoculated into 6-well plates and incubated to 80% confluence. Gently create a linear wound with a 10 μL pipette tip. The wound width was measured under light microscopy (magnification, ×100) at 0 and 24 hours later. The cell migration rate was calculated as follows: (initial width - final width)/initial width.

Colony formation assay

1.5×10^3 treated cells were seeded in six-well plates with three repetitions. After 14 days of cultivation, the colonies were washed with PBS, fixed by paraformaldehyde, and stained with 0.1% crystal violet solution for further analysis.

Virtual screening

The docking module in MOE v2015.10011 was used for structure-based virtual screening (SBVS). The X-ray structure of the protein was downloaded from RCSB Protein Data Bank (PDB ID: 6GX6) and defined as a receptor. The SPECS compounds library was selected as VS library. All compounds were prepared with the Wash module in MOE. After that all compounds were first ranked by high throughput rigid docking with London dG scoring, then the ranked top 10 K compounds were further selected to do the flexible docking with the “induced fit” protocol. Prior to docking, the force field of AMBER12: EHT and the implicit solvation model

of the Reaction Field (R-field) were selected. The protonation state of the protein and the orientation of the hydrogens were optimized by the QuickPrep module at the PH of 7 and temperature of 300 K. For flexible docking, the docked poses were ranked by London dG scoring first, then a force field refinement was carried out on the top 10 poses followed by a rescoring of GBVI/WSA dG and the best-ranked pose was retained. After flexible docking, the ranked top 100 hits were finally identified.

RNA immunoprecipitation (RIP) assay

RIP assay The RIP assay was performed with the Magna RIP kit (Merck, USA). Ovarian cancer cells were lysed overnight at 4°C in complete RIP lysis buffer containing magnetic beads conjugated with anti-IGF2BP3 or control anti-IgG antibodies. After washing the magnetic beads, the proteins were digested by incubation with proteinase K. Purified RNA was used for qRT-PCR analysis.

Co-culture assay

THP-1 cells were treated with 100 ng/ml PMA for 24 hs and induced to differentiate into adherent M0 macrophages. Then, M0 macrophages were co-cultured with A2780 cells for 48 hours to obtain tumor-associated macrophages. For co-culture experiments, A2780 cells were inoculated into the upper insert and then transferred to a 6-well plate pre-inoculated with M0 macrophages. After 48 hs, macrophages were collected for subsequent experiments.

Animal models

5-week-old female Balb/c-nu mice and C57/BL6J mice were provided by Beijing Viton Lever Laboratory Animal Technology Co. All animal experiments were approved by the animal care committee of Nanjing First Hospital, Nanjing Medical University. All mice were then grouped, and 10^6 cells (Balb/c-nu mice bearing A2780 cells and C57/BL6J mice bearing ID8 cells) were suspended in 100 μL PBS and inoculated subcutaneously. After tumor formation, tumor volumes were measured every 4 days, and subcutaneous tumor growth curves were drawn based on the measured tumor volumes. The intervention was performed when the tumor volume reached approximately 50-100 cubic centimeters. After 2 weeks of intervention treatment, mice were executed and tumors were excised and weighed. All tumors were divided into two: one was made into a single cell suspension for flow analysis; the other was paraformaldehyde fixed and made into paraffin sections for IHC analysis. The tumor volume was calculated as volume = length × width^2 × 0.5.

Statistical analysis

Statistical analysis was conducted by the SPSS software (IBM) and GraphPad Prism software (version 8). A two-sided Student's *t*-test or Mann-Whitney U-test was used for the comparison of two groups, and a parametrical or non-parametrical ANOVA test was used for multiple-comparison experiments. Survival analyses were conducted by Kaplan-Meier curve and log-rank test. $P < 0.05$ was regarded as statistically significant. All the data are shown as mean ± SD (*$P < 0.05$, **$P < 0.01$, ***$P < 0.001$, ****$P < 0.0001$).

Results

The high expression level of IGF2BP3 was associated with poor outcomes in OC patients

To investigate the role of M^{6}A-related RNA-binding protein genes in OC development, we first analyzed the mRNA expression levels of these genes using the GEPIA database. The results showed that compared with normal ovarian tissues, the mRNA expression of YTHDC1 and HNRNPA2B1 in OC tissues were lower, while the mRNA expression levels of IGF2BP2 and IGF2BP3 were higher among which the expression levels of IGF2BP3 were significant different (**Figure 1A**). However, the expressions of eIF3, HNRNPC, IGF2BP1, YTHDF1/2/3, and SRSF2 in OC were not statistically significant (Supplementary Figure 1). The expression profile of IGF2BP3 in various tumors was further analyzed by the TCGA-STAD database, and the results showed that the mRNA expression of IGF2BP3 in OC tissues was higher than that in normal tissues, and the difference was significant (**Figure 1B**). Kaplan-Meier analysis showed that high expression of IGF2BP3 predicted poor survival in OC patients (**Figure 1C**). To more accurately detect IGF2BP3 expression in OC cells, we performed single-cell sequencing and found that IGF2BP3 was

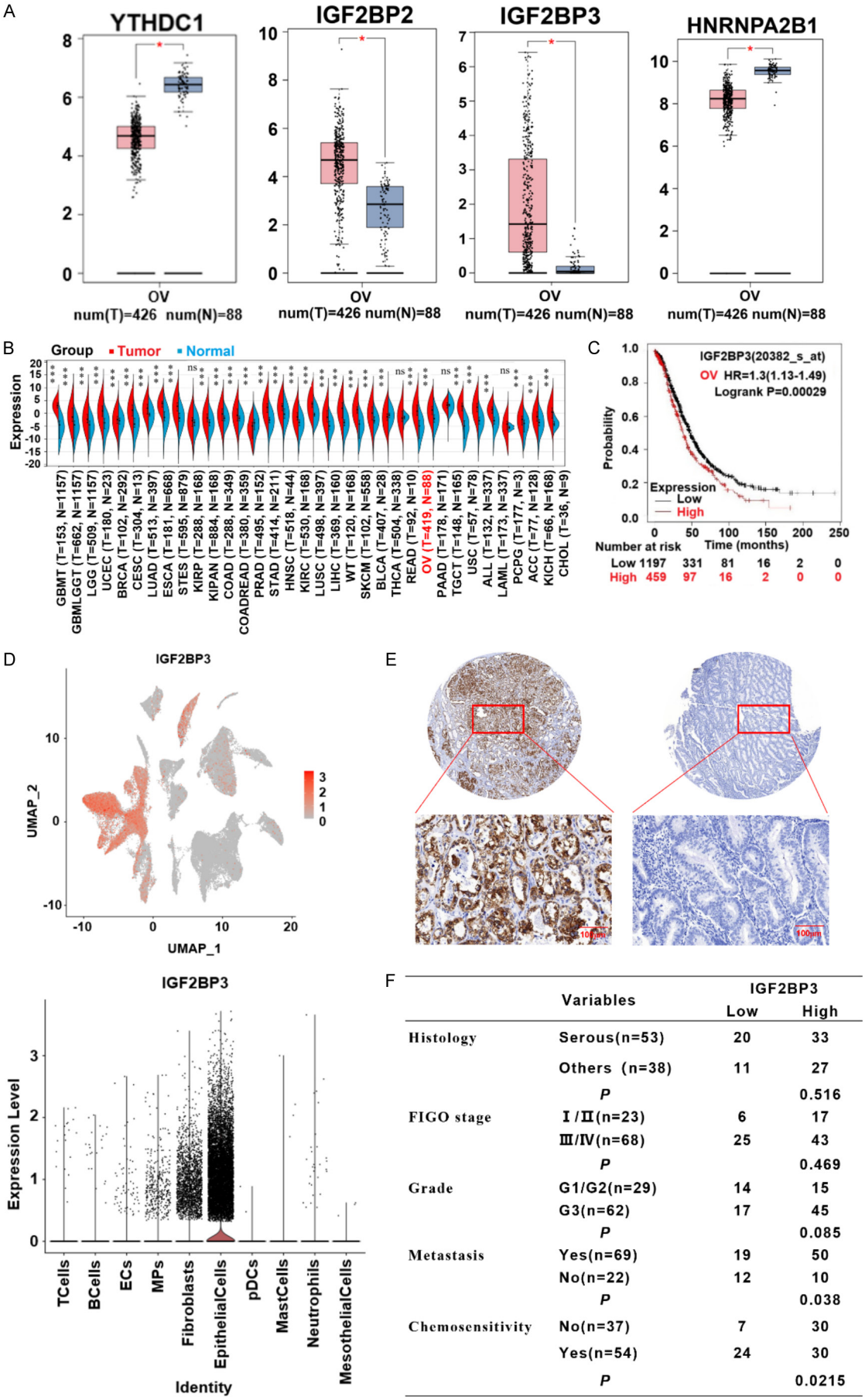

F

Variables		IGF2BP3 Low	IGF2BP3 High
Histology	Serous(n=53)	20	33
	Others (n=38)	11	27
	P		0.516
FIGO stage	Ⅰ/Ⅱ(n=23)	6	17
	Ⅲ/Ⅳ(n=68)	25	43
	P		0.469
Grade	G1/G2(n=29)	14	15
	G3(n=62)	17	45
	P		0.085
Metastasis	Yes(n=69)	19	50
	No(n=22)	12	10
	P		0.038
Chemosensitivity	No(n=37)	7	30
	Yes(n=54)	24	30
	P		0.0215

Figure 1. The high expression level of IGF2BP3 was associated with poor outcomes in OC patients. A. Analysis of the GEPIA database shows that the IGF2BP3 is highly expressed in OC tissues compared with normal tissues. B. The analysis of the TCGA-STAD database shows the expression of IGF2BP3 in various cancers. C. The Xena database analysis predicted that IGF2BP3 expression was associated with the overall survival rate of patients with OC. D. Single-cell RNA-Seq analysis reveals the expression of IGF2BP3 in ovarian cancer tissue cells. E. IHC analysis showed that IGF2BP3 was highly expressed in OC tissues compared to normal ovarian tissues. F. Analysis of IGF2BP3 levels in patients with OC concerning known prognostic factors.

highly expressed in epithelial cells, fibroblasts, and macrophages (**Figure 1D**). At the same time, we detected the protein expression level of IGF2BP3 in 91 cases of OC samples by IHC, and the results confirmed that the protein expression of IGF2BP3 protein in OC tissues was significantly higher than that in normal ovarian tissues (**Figure 1E**). The higher protein expression of IGF2BP3 protein was significantly correlated with tumor metastasis (P = 0.038) and chemotherapy sensitivity (P = 0.0215), but not with tissue type (P = 0.516), FIGO stage (P = 0.469) and G stage (P = 0.085) (**Figure 1F**). These results suggest that IGF2BP3 is highly expressed in OC cells, and can be used as a good prognostic marker and therapeutic target.

Knockdown of IGF2BP3 inhibited the malignant biological function of OC cells

To investigate the function of IGF2BP3 in OC, we overexpressed/down-regulated IGF2BP3 in OC cell lines, respectively (Supplementary Figure 2A). CCK8 assay showed that IGF2BP3 down-regulation inhibited the proliferation of A2780 and HO8910 cells (**Figure 2A**), while over-expression of IGF2BP3 induced the proliferation ability (Supplementary Figure 2B). Clone formation assay showed that IGF2BP3 down-regulation inhibited the clonal ability (**Figure 2B**), while overexpression of IGF2BP3 promoted the ability (Supplementary Figure 2C). Cell wound healing and invasion assays showed that down-regulation of IGF2BP3 impaired the migration and invasion ability of A2780 and HO8910 cells (**Figure 2C**, **2D**), whereas overexpression of IGF2BP3 promoted the migration and invasion ability of OC cells (Supplementary Figure 2D, 2E).

To investigate the regulatory mechanism of IGF2BP3, we found IGF2BP3 mRNA has a high affinity to c-MYC, CDK2, CDK6, VEGF, STAT1, and Cyclind1 mRNA through RIP-qPCR assay (**Figure 2E**) [11-15]. Both qRT-PCR and WB experiments confirmed that after IGF2BP3 knockdown, the expression of CDK2, CDK6, c-MYC, VEGF, STAT1 and Cyclind1 decreased, and vice versa (**Figure 2F**, Supplementary Figure 2A, 2F). The above results suggest that IGF2BP3 plays an important role in the proliferation, migration, and invasion of OC cells.

Development strategy for small molecule inhibitors of IGF2BP3: identification of 10 compounds

After clarifying the regulatory effect and mechanism of IGF2BP3 on OC, we targeted its structure to develop inhibitors. Select the SPECS Compound library as the virtual screening library, and **Figure 3A** shows the flow chart of structure-based virtual screening (SBVS). The compounds targeting IGF2BP3 were screened by molecular docking method, and the top 10 compounds were selected for synthesis (**Figure 3B**, Supplementary Figure 3). The OC cell line (A2780) was treated with different compounds, and the expression of related proteins was detected by WB. The results showed that AE-848 had the best effect (**Figure 3C**). We then examined the IC50 of AE-8484 in several different tumor cell lines, and also found the IC50 of AE-848 was lowest in A2780 (**Figure 3D**). To further determine the correct binding mode of AE-848, we used molecular docking to attach the structure of AE-848 to the active site of IGF2BP3. The results show that AE-848 forms stable cationic-π interaction with Arg79 and has two hydrogen bond interactions with Lys36 and Val74. In addition, it showed hydrophobic interactions with key active site residues, including Tyr39, Phe41, and Tyr5 (**Figure 3E**).

Determination of the anti-tumor effect of AE-848

IGF2BP3 has been shown to stabilize many of its target RNAs by binding to coding or non-coding sequences of mRNAs [7]. To examine whether inhibition of IGF2BP3 by AE-848 could affect its target RNA levels, the study analyzed

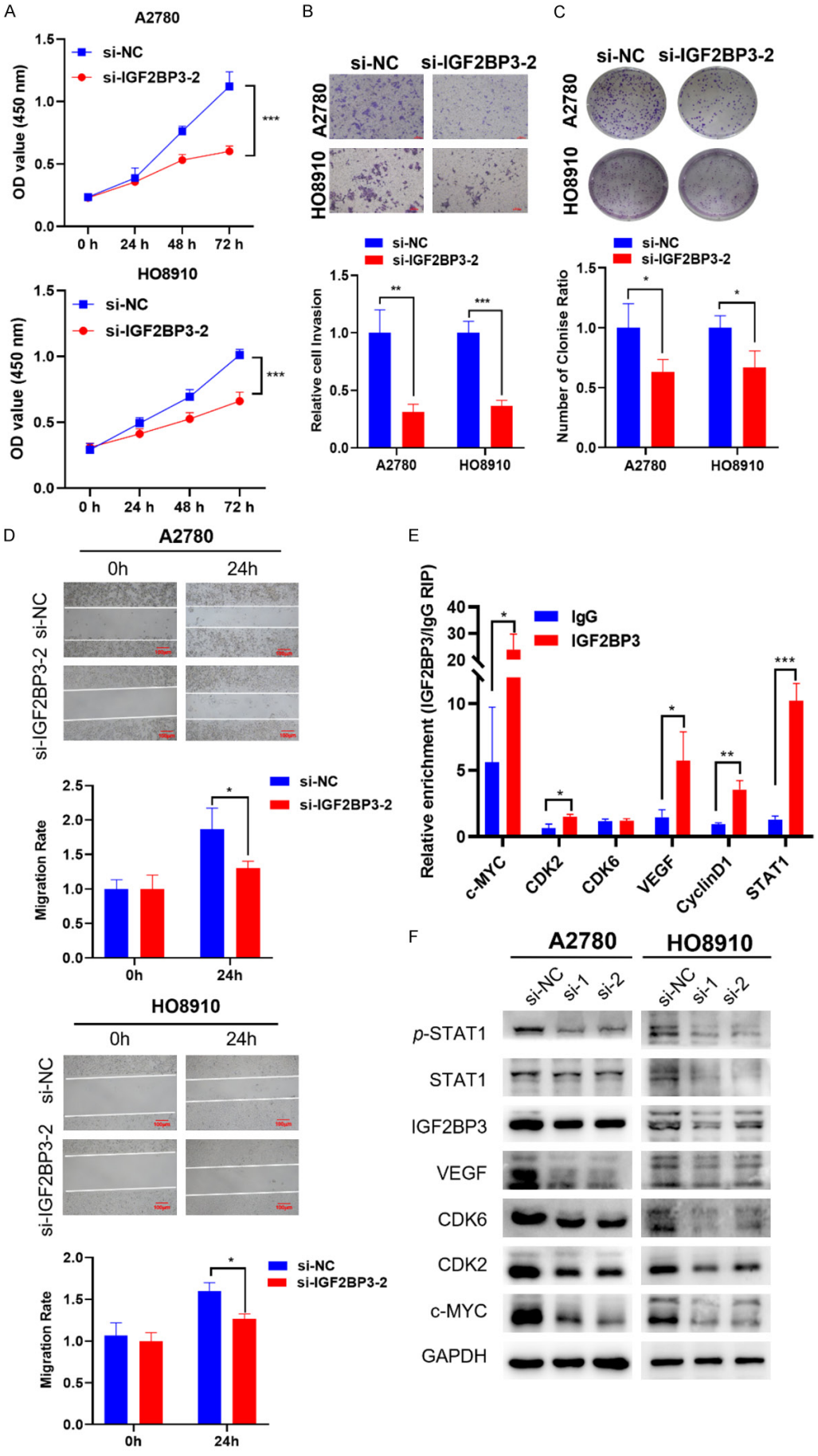
A
A2780
si-NC
si-IGF2BP3-2
OD value (450 nm)
0 h
24 h
48 h
72 h
***
HO8910
B
si-NC
si-IGF2BP3-2
A2780
HO8910
Relative cell Invasion
**
***
C
Number of Clonise Ratio
*
D
0h
24h
Migration Rate
E
IgG
IGF2BP3
Relative enrichment (IGF2BP3/IgG RIP)
c-MYC
CDK2
CDK6
VEGF
CyclinD1
STAT1
F
si-1
si-2
p-STAT1
IGF2BP3
GAPDH

Figure 2. Knockdown of IGF2BP3 inhibited the malignant biological function of OC cells. CCK8 (A), colony formation assays (B), transwell assays (C), and wound healing assays (D) of IGF2BP3 knockdown on cell proliferation, invasion, and migration. (E) The enrichment of c-MYC, CDK2, CDK6, VEGF, CyclinD1 and STAT1 mRNA by IGF2BP3 was detected by RIP-qPCR. IgG was used as a negative control. (F) Knockdown of IGF2BP3 repressed protein expression of c-MYC, CDK2, CDK6, VEGF, and STAT1 through Western Blotting assay.

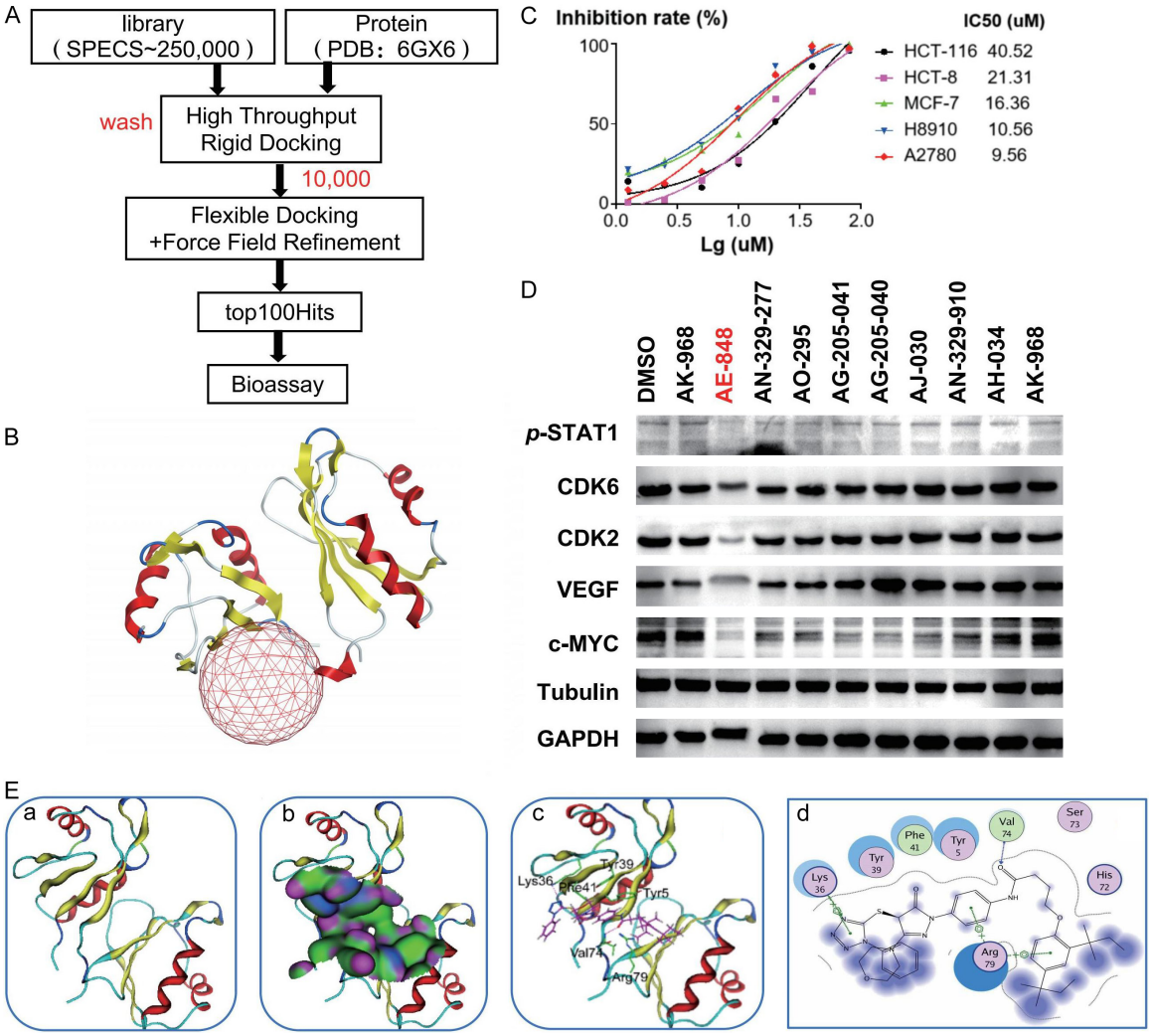

Figure 3. Development strategy for small molecule inhibitors of IGF2BP3. A. The flowchart of structure-based virtual screening. B. The binding site of protein IGF2BP3. C. Detection of the viability of various tumor cells to IGF2BP3 inhibitor AE-848 by CCK8 assay. D. The protein expression of c-MYC, CDK2, CDK6, VEGF, and STAT1 in A2780 cells was treated with AE-848 by Western blotting analysis. E. a. 3D spatial structure of IMP3. b. Molecular surfaces of the IMP3-active site. c. 3D interaction diagram of hit-1 (AE-848/33219004) bound to the active site of IMP3. The hit-1 is shown in a purple stick and active-site residues are shown in a green stick; the hydrogen bonds are shown by a red dotted line; d. 2D interaction diagram between hit-1 and active-site residues.

the expression levels of several previously identified relevant target mRNAs in A2780 cells using qRT-PCR ITGB5 and BCL2 were used as IGF2BP3 unrelated genes for negative control [16, 17]. The result showed that after incubation with AE-848 for 24 hours, the RNA levels of all genes were significantly decreased (**Figure 4A**). WB assay confirmed that the protein expression levels of c-MYC, CDK2, CDK6, VEGF, and STAT1 decreased in a dose-dependent manner after AE-848 treatment (**Figure 4B**). The effect of AE-848 on the biological function of OC cells was further detected *in vitro.* The results indicated that AE-848 could inhibit

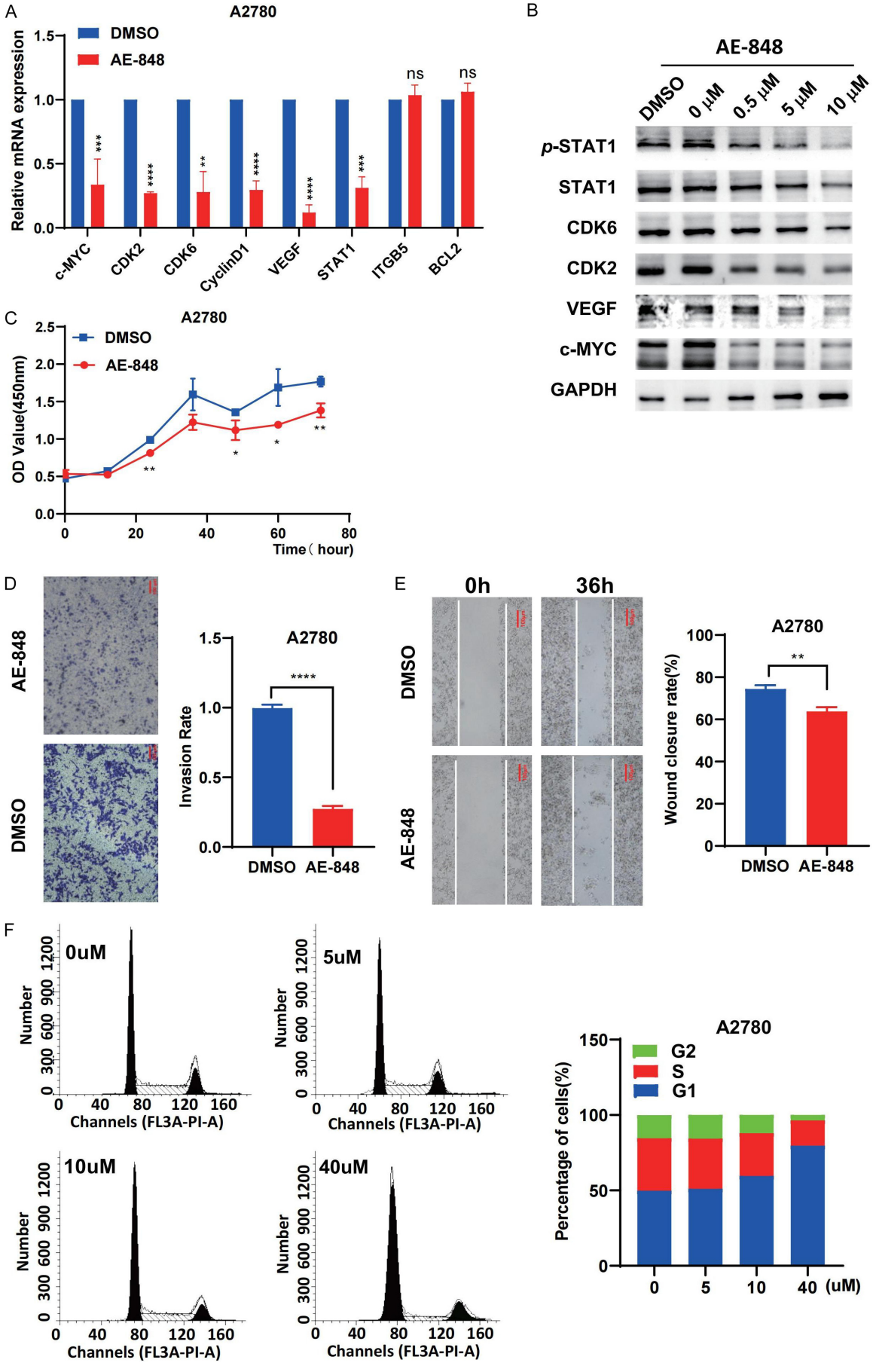
A
A2780
DMSO
AE-848
Relative mRNA expression
1.5
1.0
0.5
0.0
***
****
**
****
****
***
ns
ns
c-MYC
CDK2
CDK6
CyclinD1
VEGF
STAT1
ITGB5
BCL2
B
AE-848
DMSO
0 μM
0.5 μM
5 μM
10 μM
p-STAT1
STAT1
CDK6
CDK2
VEGF
c-MYC
GAPDH
C
A2780
DMSO
AE-848
OD Value(450nm)
2.5
2.0
1.5
1.0
0.5
0.0
**
*
*
**
0
20
40
60
80
Time (hour)
D
AE-848
DMSO
A2780
Invasion Rate
1.5
1.0
0.5
0.0
****
DMSO
AE-848
E
0h
36h
DMSO
AE-848
A2780
Wound closure rate(%)
100
80
60
40
20
0
**
DMSO
AE-848
F
0uM
5uM
10uM
40uM
Number
1200
900
600
300
0
0
40
80
120
160
Channels (FL3A-PI-A)
A2780
Percentage of cells(%)
150
100
50
0
G2
S
G1
0
5
10
40
(uM)

Figure 4. Determination of the anti-tumor effect of AE-848 (10 μM). (A) qRT-PCR analysis of the mRNA expression level of IGF2BP3 target RNA in A2780 cells treated with AE-848. (B) Western Blotting analysis of c-MYC, CDK2, CDK6, VEGF, and STAT1 protein expression in A2780 cells treated with different concentrations of AE-848. CCK8 (C), transwell assays (D), and wound healing assays (E) of cell proliferation, invasion, and migration treated with AE-848. (F) Flow cytometric analysis of changes in the cell cycle profile of A2780 cells treated with different concentrations of AE-848.

the proliferation, migration, and invasion ability of OC cell line (**Figure 4C-E**). In addition, the flow cytometry results showed that the cells in G0/G1 phase were significantly increased while decreased in S phase after using AE-848 (**Figure 4F**).

AE-848 inhibits the growth of OC cells in vivo

The inhibitory effect of AE-848 on OC was evaluated using a subcutaneous tumor model. A total of 15 subcutaneous tumor models were randomly divided into three groups: PBS, DDP (2 mg/kg), and AE-848 (20 mg/kg) (n = 5). As shown in Supplementary Figure 4A-C, AE-848 inhibited the growth of OC cell xenografts. IHC assay results showed that the expression level of Ki-67 in the AE-848 group was significantly lower than that in the PBS control group and DDP treatment group (Supplementary Figure 4D). To further verify the anti-tumor effect of different doses of AE-848, ID8 cells (mouse OC cell line) were implanted subcutaneously into immune healthy mice to form tumors (**Figure 5A**). Twenty subcutaneous tumor models were randomly divided into PBS, DDP, AE-848 (low-dose group, 20 mg/kg), and AE-848 (high-dose group, 40 mg/kg) groups (n = 5). Compared with the PBS group, both doses group of AE-848 showed delayed tumor growth; while compared with the DDP group, the AE-848 (40 mg/kg) group achieved a better therapeutic effect (**Figure 5B-D**). The IHC results showed that AE-848 inhibited the protein expression levels of c-MYC, CDK2, and VEGF proteins; meanwhile, the expression levels of Ki-67 in the AE-848 group were significantly lower than those in the PBS and DDP groups (**Figure 5E**).

In this study, the effect of AE-848 on the immune microenvironment of OC was analyzed by flow cytometry. The analysis showed that the number of macrophages was significantly increased in the AE-848 (40 mg/kg) group compared to other groups, and most of them were M1 macrophages, while the number of T cells and Treg cells did not change significantly in the different groups (**Figure 5F**, Supplementary Figure 4E, 4F). Further testing of serum cytokines in each group of tumor-bearing mice showed increased levels of INF-γ and TNF-α in the AE-848 (40 mg/kg) group (**Figure 5G**). In conclusion, these results showed that systemic therapy with AE-848 significantly inhibited tumor growth by reducing the expression of tumor-associated antigen (c-MYC/VEGF/Ki67/CDK2) and promote to secret INF-γ and TNF-α.

Roles of AE-848 on macrophage polarization

In the complex tumor microenvironment (TME), tumor-associated macrophages (TAMs) are phenotypically alternatively M1-M2 polarized [18], and c-MYC is a key molecule for IL-4-induced M2 macrophage activation [19]. Our results revealed that the percentage of M1-type macrophages was increased in the tumor tissues of the AE-848 group; meanwhile, the expression levels of pro-inflammatory factors were elevated. Therefore, we further investigated the roles of AE-848 on macrophage polarization.

As shown in **Figure 6A**, **6B**, AE-848 can reverse the highly expressed c-MYC levels in M2 macrophages induced by IL-4 (20 ng/ml) and IL-13 (20 ng/ml) and inhibit the M2 type cytokine (Arg-1 and CCL2) expression. Due to the complexity of the TME, we co-cultured M0 macrophages with A2780 cells for 48 h to make them TAMs. TAMs were incubated with AE-848 and DMSO for 24 h, respectively. It was found that the mRNA expression of c-MYC in TAMs decreased under the AE-848 treatment, while the mRNA expression of inflammatory factors such as INF-γ and TNF-α increased (**Figure 6C**). These results were also confirmed at protein levels (**Figure 6D**, **6E**). In conclusion, this study revealed that AE-848 blocked the polarization of TMAs to M2-type macrophages by inhibiting the expression of c-MYC, thus enhancing the anti-tumor effect of macrophages.

Discussion

IGF2BPs protein is part of the m^6A reader, which is upregulated in many tumors and fre-

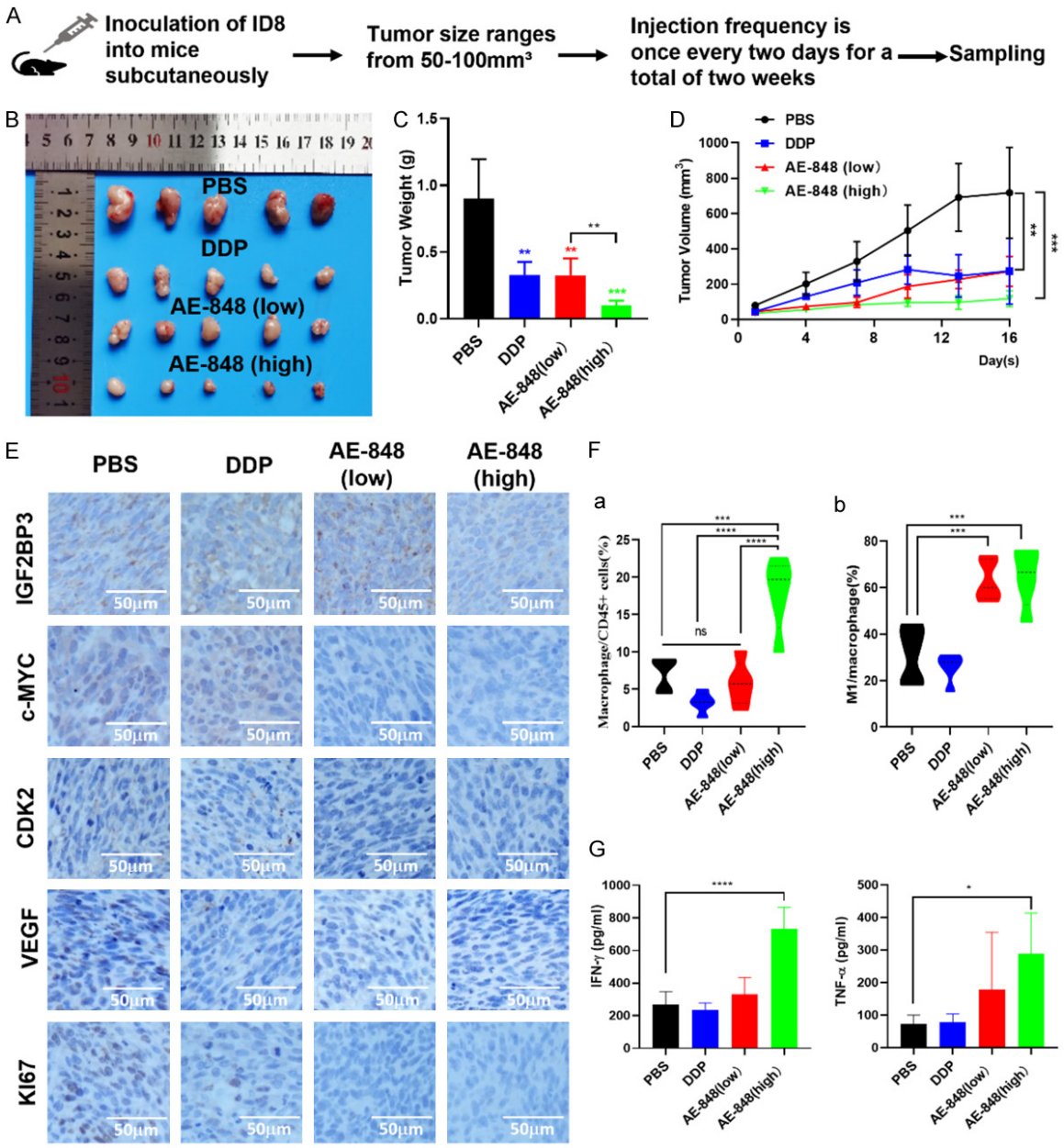

Figure 5. AE-848 inhibits the growth of OC cells *in vivo*. (A) Diagram of the experiment. (B) Tumors of ID8 xenograft treated with PBS, DDP, or AE-848 (20 or 40 mg/kg/2 days intraperitoneally) for 2 weeks. The ruler scale is in centimeters. (C) Growth curve of tumor of mice treated with PBS, DDP, or AE-848. (D) Comparison of the weight of tumors in four treatment groups of mice. (E) The expression of IGF2BP3, c-MYC, CDK2, VEGF, and Ki-67 in tumors detected by IHC. (F) The fractions of tumoral macrophage cells (a) and the proportion of M1 type in macrophages (b). (G) Levels of INF-γ and TNF-α in the serum of each group of mice.

quently associated with oncogenic behavior [20]. Recent studies have shown that IGF2BP3 is involved in regulating the development of a variety of cancers and is associated with drug resistance [15, 21-25]. Hsu et al found that high expression of IGF2BP3 reduced OC cells' sensitivity to cisplatin and reduced patient survival. This is consistent with our findings that IGF2BP3 is highly expressed in OC cells and is associated with chemotherapy sensitivity and poor prognosis.

At present, no small molecule inhibitors targeting IGF2BP3 have been reported. In this study, AE-848, a small molecule inhibitor targeting IGF2BP3, was screened by the small molecule

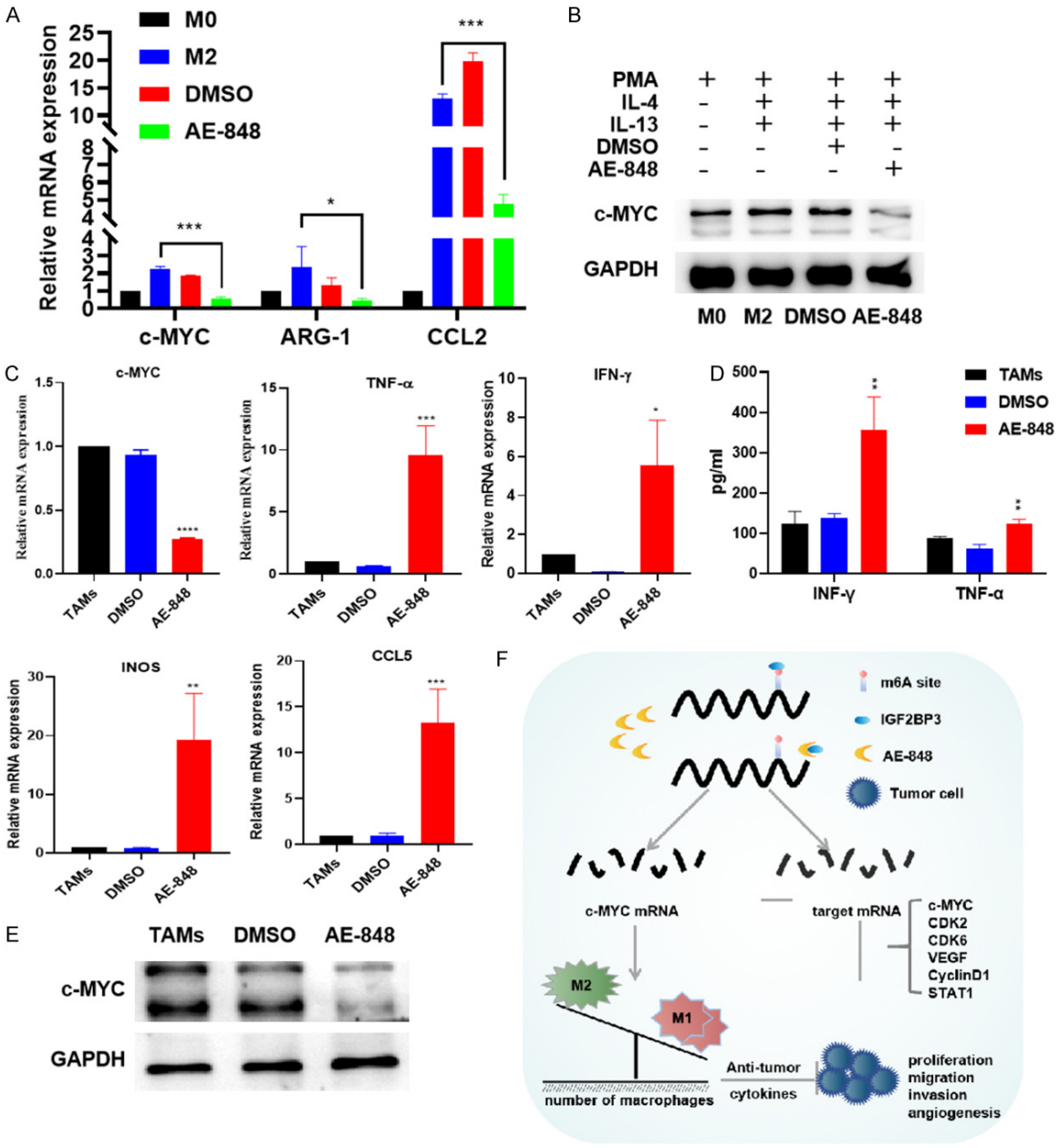

Figure 6. Roles of AE-848 on macrophage polarization. A. The mRNA expression of ARG-1, CCL2, and c-MYC were detected by qRT-PCR in THP-1-M0, THP-1-M0 treated with IL-4 and IL-13, THP-1-M0 treated with IL-4, IL-13, and DMSO, THP-1-M0 treated with IL-4, IL-13, and AE-848. B. Detection of c-MYC protein by Western blotting in THP-1-M0, THP-1-M0 treated with IL-4 and IL-13, THP-1-M0 treated with IL-4, IL-13, and DMSO, THP-1-M0 treated with IL-4, IL-13, and AE-848. C. The mRNA expression of relevant cytokines in DMSO (or AE-848)-treated TAMs by qRT-PCR. D. Levels of INF-γ and TNF-α in culture medium TAMs treated with DMSO or AE-848. E. Detection of c-MYC protein by Western blotting in TAMs treated with DMSO or AE-848. F. Mechanism of anti-tumor effect of AE-848.

docking method, and further verified *in vitro* and *in vivo*. AE-848 attenuates the stability of its binding target RNA by binding IGF2BP3 during incubation with OC cells. AE-848 can reduce c-MYC and other target mRNAs, such as VEGF, CyclinD1, CDK2, and STAT1; and inhibit the protein expression level of c-MYC, VEGF, CDK6, CDK2, and STAT1. In turn, it inhibited tumor cell migration, invasion, and proliferation. *In vivo*, AE-848 also showed potent anti-tumor effects, increasing the proportion of M1 tumor-associated macrophages in the TME and stimulating the secretion of pro-inflammatory factors.

MYC oncogene (also known as c-MYC), acts as a transcription factor that regulates the expression of thousands of genes and exerts various effects on cellular programs, including changes in tumor cell-intrinsic biology, host immunity, and TME [26]. C-MYC gene amplification is found in many solid tumor types, especially in ovarian adenocarcinoma and uterine carcinosarcoma [26]. However, the nuclear localization of the c-MYC gene and its lack of a well-defined ligand binding sites make it extremely difficult to develop drugs that directly target c-MYC proteins. IGF2BP3 is induced by the oncogene c-MYC, and IGF2BP3 increases c-MYC mRNA and protein levels by stabilizing c-MYC mRNA, which is a tumor-promoting feedforward regulatory circuit [14, 27]. It is therefore challenging to break this cancer-causing feedforward regulatory ring with c-MYC inhibitors, which allow IGF3BP2 inhibitors to reduce c-MYC protein levels by reducing their mRNA stability.

In addition, it has been reported that the selective polarization of macrophages requires the transcription factor c-MYC, but IFN-γ and TNF-α can reduce c-MYC transcription through different molecular mechanisms, while classically activated M1 macrophages are dependent on IFN-γ activation [19, 28, 29]. Reduced levels of c-MYC expression level and elevated levels of IFN-γ promote a higher proportion of M1-type TAMs, which in turn M1-type macrophages have pro-inflammatory functions, enhanced antigen presentation, induction of cytotoxic T lymphocyte (CTL) activity in $CD8^+$ T cells, and direct tumor-killing activity, all of which promote the immune elimination of tumors [30].

Our experiments verified that several other IGF2BP3 target mRNAs (VEGF, CDK2/CDK6, and STAT1) were reduced in ovarian cancer cells treated with IGF2BP3 inhibitor AE-848. These results are consistent with the fact that IGF2BP3 promotes a proto-oncogene phenotype based on its ability to bind many mRNAs associated with tumor cells [31, 32]. VEGF is an important molecule in ovarian cancer, and its expression is negatively correlated with the prognosis of ovarian cancer patients [33]. Therefore, anti-angiogenic therapy targeting VEGF is one of the important treatment strategies for advanced ovarian cancer. Cell cycle protein-dependent kinase 2 (CDK2) is a potential therapeutic target for cancer treatment, and the antiproliferative activity of ovarian cancer cells depends on the degradation of CDK2 [34]. CDK6 impairs the sensitivity of ovarian cancer cells to platinum by upregulating FOXO3, and the combination of CDK4/6 inhibitors and anti-PD1 antibodies improves the efficacy of anti-PD1 therapy [35, 36]. Signal transducer and activator of transcription 1 (STAT1), as a transcription factor and trans-activator protein, STAT1 can regulate its target genes or be a target gene regulated by other molecules, so its role in ovarian cancer is not fully understood and needs to be further explored [37]. In conclusion, these findings coincide with our study. These suggest that the anti-tumor effect of AE-848 may also be related to anti-angiogenesis, inhibition of cell cycle, and reversal of tumor drug resistance, which needs further exploration in the follow-up study.

We present a proof of concept here that AE-848, a small molecule that targets oncogenic IGF2BP3 and affects related signaling pathways, could be an effective therapeutic strategy for the treatment of the ovarian cancer (**Figure 6F**). Therefore, we envision that optimized small molecules based on AE-848 may be useful in clinical settings, either as monotherapy for cancer progression, cell migration and metastasis formation, or as adjuvant therapy in combination with chemotherapy drugs. Since IGF2BP3 also affects the progression of other tumors, we expect that further refinement of compounds like AE-848 will lead to a new class of drugs that may also have broad implications for the treatment of tumors other than ovarian cancer.

Acknowledgements

We acknowledge the support from the National Natural Science Foundation of China (grant numbers: 82273196 and 82173205), the Key Research and Development Program of Jiangsu Province (grant number: BE2019617), and six peak talents of Jiangsu Province (grant number: SWYY-170).

Disclosure of conflict of interest

None.

Address correspondence to: Shu-Li Zhao, General Clinical Research Center, Nanjing First Hospital,

China Pharmaceutical University, 68 Changle Road, Nanjing 210006, Jiangsu, China. Tel: +86-153-6613-6120; E-mail: shulizhao79@njmu.edu.cn; Wei Zhao, Department of Pathology, Nanjing First Hospital, Nanjing Medical University, 68 Changle Road, Nanjing 210006, Jiangsu, China. Tel: +86-180-1332-0837; E-mail: zhaowei_njmu@163.com

References

[1] Siegel RL, Miller KD, Fuchs HE and Jemal A. Cancer statistics, 2022. CA Cancer J Clin 2022; 72: 7-33.

[2] Yang WL, Lu Z and Bast RC Jr. The role of biomarkers in the management of epithelial ovarian cancer. Expert Rev Mol Diagn 2017; 17: 577-591.

[3] Kuroki L and Guntupalli SR. Treatment of epithelial ovarian cancer. BMJ 2020; 371: m3773.

[4] Moufarrij S, Dandapani M, Arthofer E, Gomez S, Srivastava A, Lopez-Acevedo M, Villagra A and Chiappinelli KB. Epigenetic therapy for ovarian cancer: promise and progress. Clin Epigenetics 2019; 11: 7.

[5] Nielsen J, Christiansen J, Lykke-Andersen J, Johnsen AH, Wewer UM and Nielsen FC. A family of insulin-like growth factor II mRNA-binding proteins represses translation in late development. Mol Cell Biol 1999; 19: 1262-1270.

[6] Huang H, Weng H, Sun W, Qin X, Shi H, Wu H, Zhao BS, Mesquita A, Liu C, Yuan CL, Hu YC, Hüttelmaier S, Skibbe JR, Su R, Deng X, Dong L, Sun M, Li C, Nachtergaele S, Wang Y, Hu C, Ferchen K, Greis KD, Jiang X, Wei M, Qu L, Guan JL, He C, Yang J and Chen J. Recognition of RNA N(6)-methyladenosine by IGF2BP proteins enhances mRNA stability and translation. Nat Cell Biol 2018; 20: 285-295.

[7] Yang Y, Hsu PJ, Chen YS and Yang YG. Dynamic transcriptomic m(6)A decoration: writers, erasers, readers and functions in RNA metabolism. Cell Res 2018; 28: 616-624.

[8] Liu H, Zeng Z, Afsharpad M, Lin C, Wang S, Yang H, Liu S, Kelemen LE, Xu W, Ma W, Xiang Q, Mastriani E, Wang P, Wang J, Liu SL, Johnston RN and Köbel M. Overexpression of IGF2BP3 as a potential oncogene in ovarian clear cell carcinoma. Front Oncol 2020; 9: 1570.

[9] Köbel M, Xu H, Bourne PA, Spaulding BO, Shih IeM, Mao TL, Soslow RA, Ewanowich CA, Kalloger SE, Mehl E, Lee CH, Huntsman D and Gilks CB. IGF2BP3 (IMP3) expression is a marker of unfavorable prognosis in ovarian carcinoma of clear cell subtype. Mod Pathol 2009; 22: 469-475.

[10] Zhang Y, Rong D, Li B and Wang Y. Targeting epigenetic regulators with covalent small-molecule inhibitors. J Med Chem 2021; 64: 7900-7925.

[11] Hoefig KP, Reim A, Gallus C, Wong EH, Behrens G, Conrad C, Xu M, Kifinger L, Ito-Kureha T, Defourny KAY, Geerlof A, Mautner J, Hauck SM, Baumjohann D, Feederle R, Mann M, Wierer M, Glasmacher E and Heissmeyer V. Defining the RBPome of primary T helper cells to elucidate higher-order roquin-mediated mRNA regulation. Nat Commun 2021; 12: 5208.

[12] Jian Y, Huang X, Fang L, Wang M, Liu Q, Xu H, Kong L, Chen X, Ouyang Y, Wang X, Wei W and Song L. Actin-like protein 6A/MYC/CDK2 axis confers high proliferative activity in triple-negative breast cancer. J Exp Clin Cancer Res 2021; 40: 56.

[13] Mäkinen A, Nikkilä A, Haapaniemi T, Oksa L, Mehtonen J, Vänskä M, Heinäniemi M, Paavonen T and Lohi O. IGF2BP3 associates with proliferative phenotype and prognostic features in B-cell acute lymphoblastic leukemia. Cancers (Basel) 2021; 13: 1505.

[14] Palanichamy JK, Tran TM, Howard JM, Contreras JR, Fernando TR, Sterne-Weiler T, Katzman S, Toloue M, Yan W, Basso G, Pigazzi M, Sanford JR and Rao DS. RNA-binding protein IGF2BP3 targeting of oncogenic transcripts promotes hematopoietic progenitor proliferation. J Clin Invest 2016; 126: 1495-1511.

[15] Yang Z, Wang T, Wu D, Min Z, Tan J and Yu B. RNA N6-methyladenosine reader IGF2BP3 regulates cell cycle and angiogenesis in colon cancer. J Exp Clin Cancer Res 2020; 39: 203.

[16] Anisimova AS and Karagöz GE. Optimized infrared photoactivatable ribonucleoside-enhanced crosslinking and immunoprecipitation (IR-PAR-CLIP) protocol identifies novel IGF2BP3-interacting RNAs in colon cancer cells. RNA 2023; [Epub ahead of print].

[17] Conway AE, Van Nostrand EL, Pratt GA, Aigner S, Wilbert ML, Sundararaman B, Freese P, Lambert NJ, Sathe S, Liang TY, Essex A, Landais S, Burge CB, Jones DL and Yeo GW. Enhanced CLIP uncovers IMP protein-RNA targets in human pluripotent stem cells important for cell adhesion and survival. Cell Rep 2016; 15: 666-679.

[18] Zhou K, Cheng T, Zhan J, Peng X, Zhang Y, Wen J, Chen X and Ying M. Targeting tumor-associated macrophages in the tumor microenvironment. Oncol Lett 2020; 20: 234.

[19] Pello OM, De Pizzol M, Mirolo M, Soucek L, Zammataro L, Amabile A, Doni A, Nebuloni M, Swigart LB, Evan GI, Mantovani A and Locati M. Role of c-MYC in alternative activation of human macrophages and tumor-associated macrophage biology. Blood 2012; 119: 411-421.

[20] Wang S, Chai P, Jia R and Jia R. Novel insights on m(6)A RNA methylation in tumorigenesis: a double-edged sword. Mol Cancer 2018; 17: 101.
[21] Kim HY, Ha Thi HT and Hong S. IMP2 and IMP3 cooperate to promote the metastasis of triple-negative breast cancer through destabilization of progesterone receptor. Cancer Lett 2018; 415: 30-39.
[22] Lederer M, Bley N, Schleifer C and Hüttelmaier S. The role of the oncofetal IGF2 mRNA-binding protein 3 (IGF2BP3) in cancer. Semin Cancer Biol 2014; 29: 3-12.
[23] Li Y, Xiao J, Bai J, Tian Y, Qu Y, Chen X, Wang Q, Li X, Zhang Y and Xu J. Molecular characterization and clinical relevance of m(6)A regulators across 33 cancer types. Mol Cancer 2019; 18: 137.
[24] Zhang N, Shen Y, Li H, Chen Y, Zhang P, Lou S and Deng J. The m^6A reader IGF2BP3 promotes acute myeloid leukemia progression by enhancing RCC2 stability. Exp Mol Med 2022; 54: 194-205.
[25] Zhang Z, Zhang C, Yang Z, Zhang G, Wu P, Luo Y, Zeng Q, Wang L, Xue Q, Zhang Y, Sun N and He J. m(6)A regulators as predictive biomarkers for chemotherapy benefit and potential therapeutic targets for overcoming chemotherapy resistance in small-cell lung cancer. J Hematol Oncol 2021; 14: 190.
[26] Dhanasekaran R, Deutzmann A, Mahauad-Fernandez WD, Hansen AS, Gouw AM and Felsher DW. The MYC oncogene - the grand orchestrator of cancer growth and immune evasion. Nat Rev Clin Oncol 2022; 19: 23-36.
[27] Du M, Peng Y, Li Y, Sun W, Zhu H, Wu J, Zong D, Wu L and He X. MYC-activated RNA N6-methyladenosine reader IGF2BP3 promotes cell proliferation and metastasis in nasopharyngeal carcinoma. Cell Death Discov 2022; 8: 53.
[28] Yarden A and Kimchi A. Tumor necrosis factor reduces c-myc expression and cooperates with interferon-gamma in HeLa cells. Science 1986; 234: 1419-1421.
[29] Sica A and Mantovani A. Macrophage plasticity and polarization: in vivo veritas. J Clin Invest 2012; 122: 787-795.
[30] Noy R and Pollard JW. Tumor-associated macrophages: from mechanisms to therapy. Immunity 2014; 41: 49-61.
[31] Folkman J, Merler E, Abernathy C and Williams G. Isolation of a tumor factor responsible for angiogenesis. J Exp Med 1971; 133: 275-288.
[32] He L, Zhu W, Chen Q, Yuan Y, Wang Y, Wang J and Wu X. Ovarian cancer cell-secreted exosomal miR-205 promotes metastasis by inducing angiogenesis. Theranostics 2019; 9: 8206-8220.
[33] Chen Y, Zhang L, Liu WX and Wang K. VEGF and SEMA4D have synergistic effects on the promotion of angiogenesis in epithelial ovarian cancer. Cell Mol Biol Lett 2018; 23: 2.
[34] Teng M, Jiang J, He Z, Kwiatkowski NP, Donovan KA, Mills CE, Victor C, Hatcher JM, Fischer ES, Sorger PK, Zhang T and Gray NS. Development of CDK2 and CDK5 dual degrader TMX-2172. Angew Chem Int Ed Engl 2020; 59: 13865-13870.
[35] Dall'Acqua A, Sonego M, Pellizzari I, Pellarin I, Canzonieri V, D'Andrea S, Benevol S, Sorio R, Giorda G, Califano D, Bagnoli M, Militello L, Mezzanzanica D, Chiappetta G, Armenia J, Belletti B, Schiappacassi M and Baldassarre G. CDK6 protects epithelial ovarian cancer from platinum-induced death via FOXO3 regulation. EMBO Mol Med 2017; 9: 1415-1433.
[36] Zhang QF, Li J, Jiang K, Wang R, Ge JL, Yang H, Liu SJ, Jia LT, Wang L and Chen BL. CDK4/6 inhibition promotes immune infiltration in ovarian cancer and synergizes with PD-1 blockade in a B cell-dependent manner. Theranostics 2020; 10: 10619-10633.
[37] Li X, Wang F, Xu X, Zhang J and Xu G. The dual role of STAT1 in ovarian cancer: insight into molecular mechanisms and application potentials. Front Cell Dev Biol 2021; 9: 636595.

Supplementary Table 1. The Primers for RT-qPCR

Gene	Forward Primer	Reverse Primer
c-MYC	GGACCTTCTGACCACGAT	GCAACAGCATAACGCCTC
CDK6	GCTGACCAGCAGTACGAATG	GCACACATCAAACAACCTGACC
Cyclin D1	CCGCACGATTTCATTGAACACT	CGAAGGTCTGCGCGTGTTT
CDK2	CCAGGAGTTACTTCTATGCCTGA	TTCATCCAGGGGAGGTACAAC
VEGF	CGGTCCCTCTTGGAATTGGA	TTCCCCTCCCAACTCAAGTC
STAT1	TGTGAAGTTGAGAGATGTGAATGA	TTGGAGATCACCACAACGGG
GAPDH	GAGAAGGCTGGGGCTCATTT	AGTGATGGCATGGACTGTGG
IGF2BP3	CGGTCCCAAAAAGGCAAAGG	TCCCACTGTAAATGAGGCGG
ITGB5	GCAGATACCTTTGGCCCCTT	TGGGACGTAAGTGTTTCGGG
BCL2	GGATAACGGAGGCTGGGATG	TGACTTCACTTGTGGCCCAG

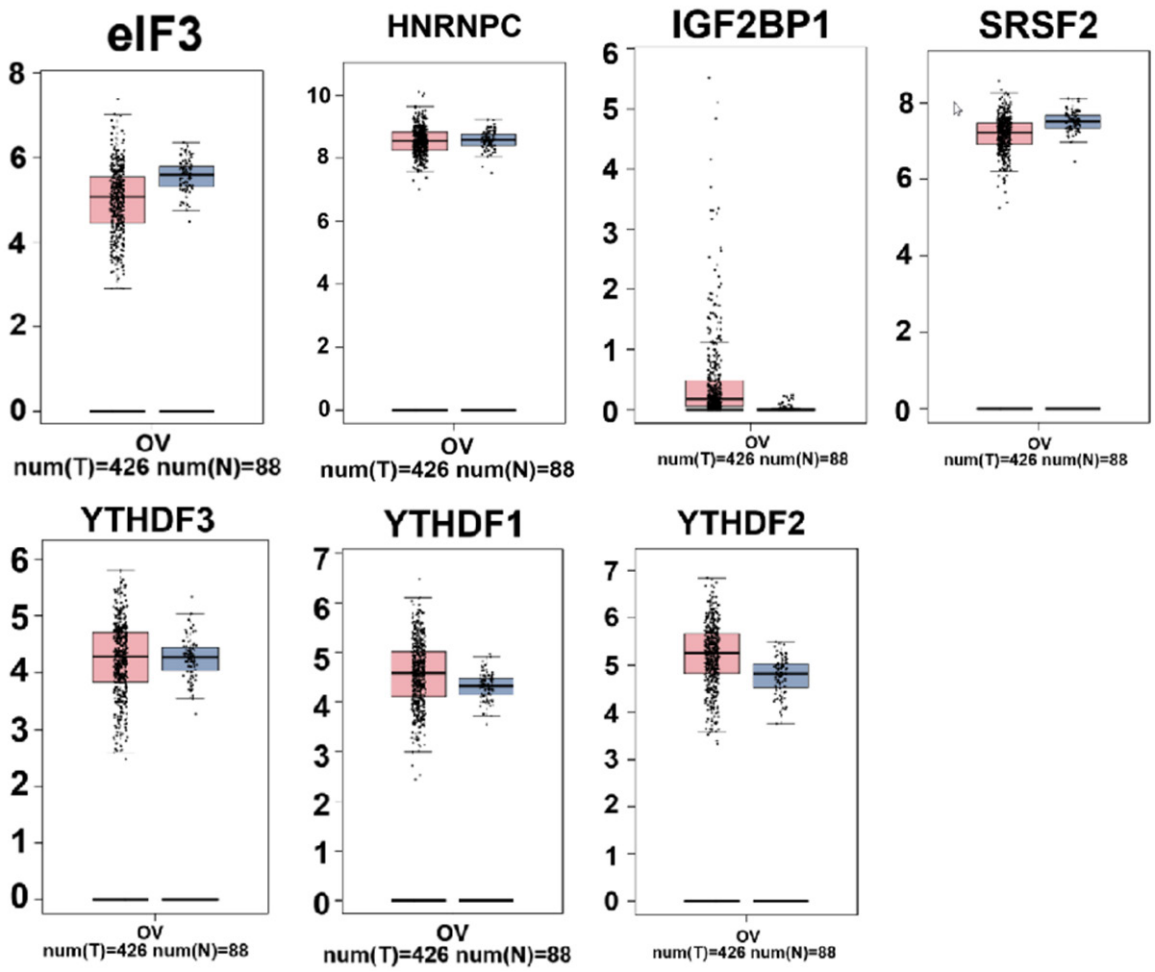

Supplementary Figure 1. Analysis of the GEPIA database showed that m^{6}A methylated reading protein was expressed in OC tissues compared to normal tissue.

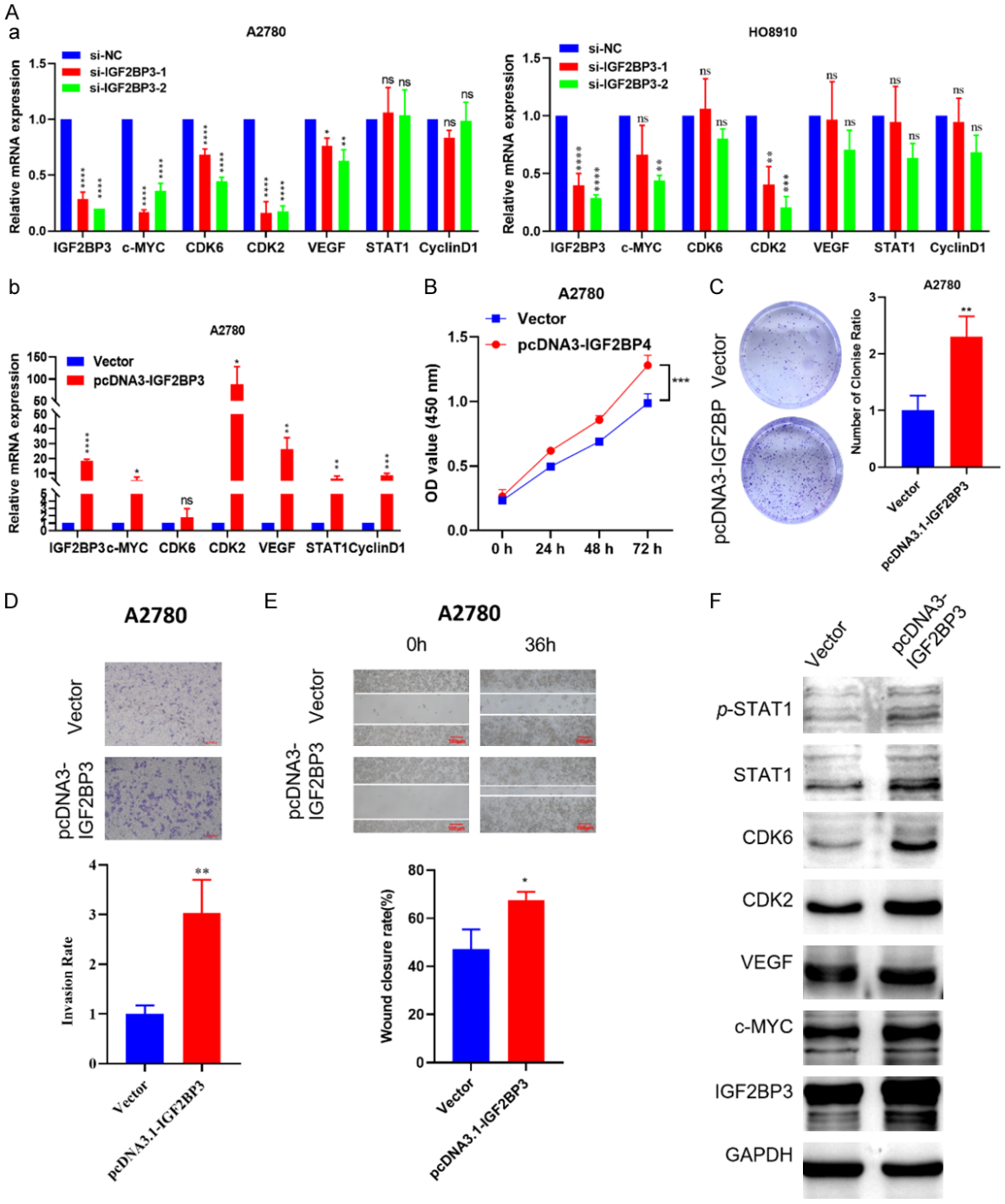

Supplementary Figure 2. (A) qRT-PCR analysis of mRNA expression in two OC cell lines transfected with two specific IGF2BP3 siRNAs (a); qRT-PCR analysis of mRNA expression in A2780 cell transfected with IGF2BP3-overexpressing plasmid (b). CCK8 (B), colony formation assays (C), transwell assays (D), and wound healing assays (E) of IGF2BP3 overexpressed on A2780 cell proliferation, invasion, and migration. (F) Overexpression of IGF2BP3 repressed protein expression of c-MYC, CDK2, CDK6, VEGF, and STAT1 confirmed by Western Blotting analysis.

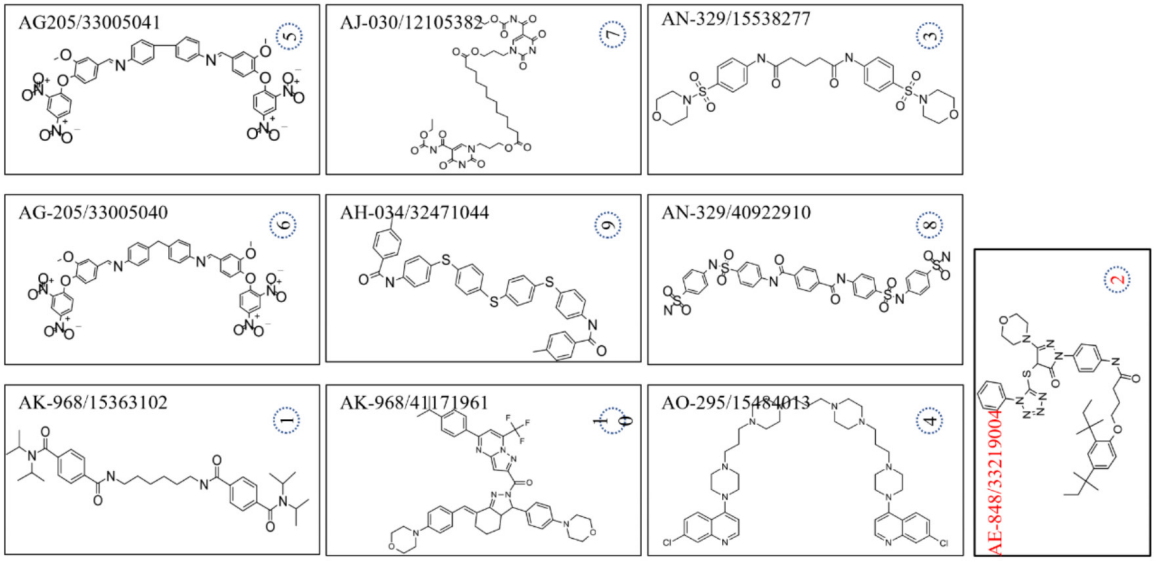

Supplementary Figure 3. Chemical structures of ten small molecule compounds.

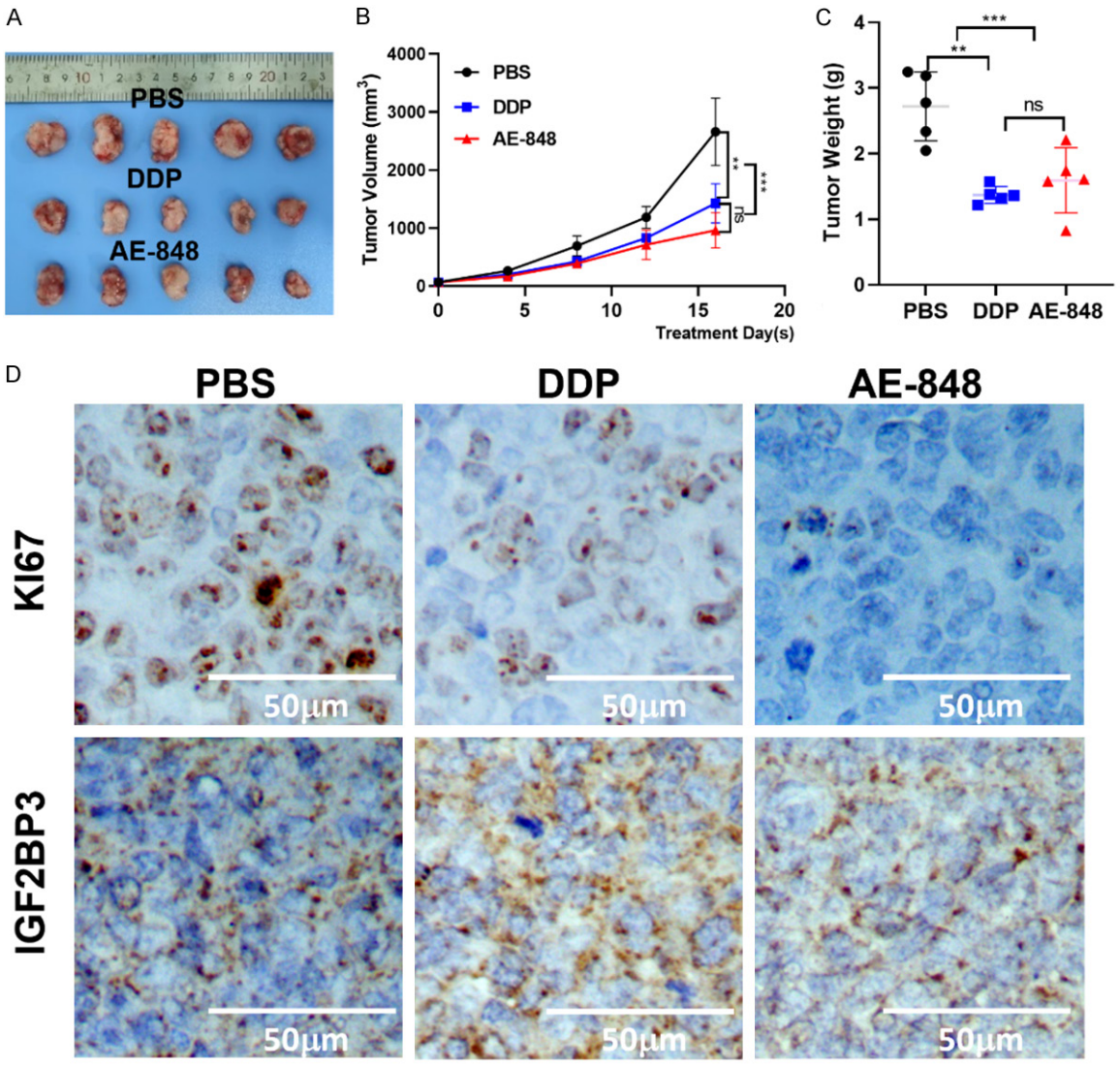

E

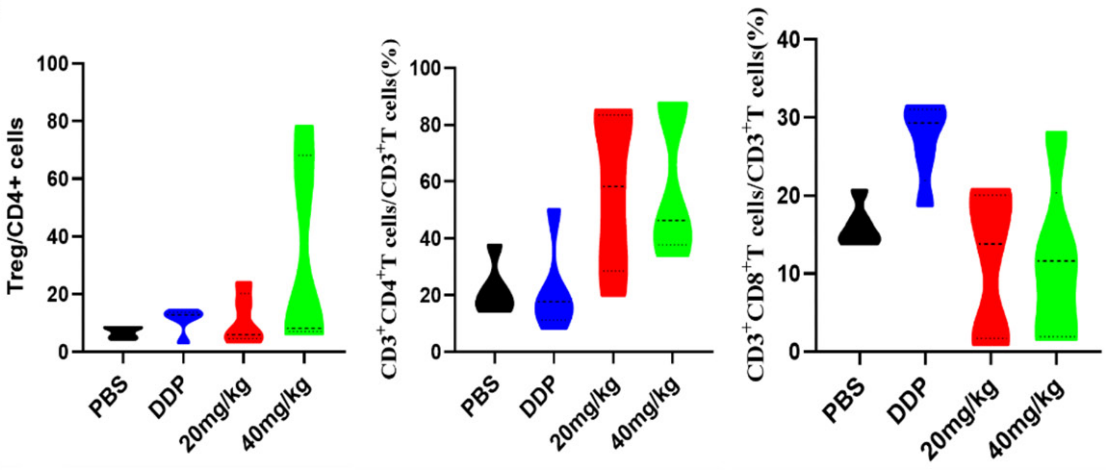
Treg/CD4+ cells
100
80
60
40
20
0
PBS
DDP
20mg/kg
40mg/kg
CD3+CD4+T cells/CD3+T cells(%)
100
80
60
40
20
0
PBS
DDP
20mg/kg
40mg/kg
CD3+CD8+T cells/CD3+T cells(%)
40
30
20
10
0
PBS
DDP
20mg/kg
40mg/kg

F

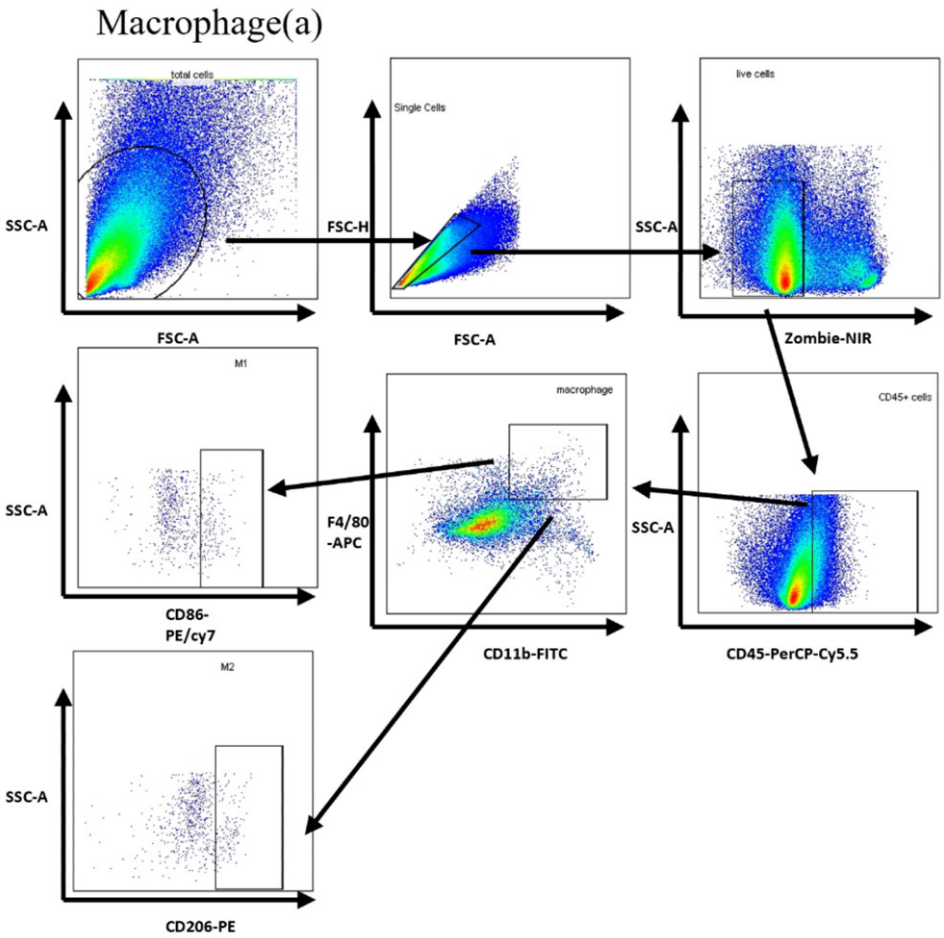
Macrophage(a)
total cells
SSC-A
FSC-A
Single Cells
FSC-H
FSC-A
live cells
SSC-A
Zombie-NIR
M1
SSC-A
CD86-
PE/cy7
macrophage
F4/80
-APC
CD11b-FITC
CD45+ cells
SSC-A
CD45-PerCP-Cy5.5
M2
SSC-A
CD206-PE

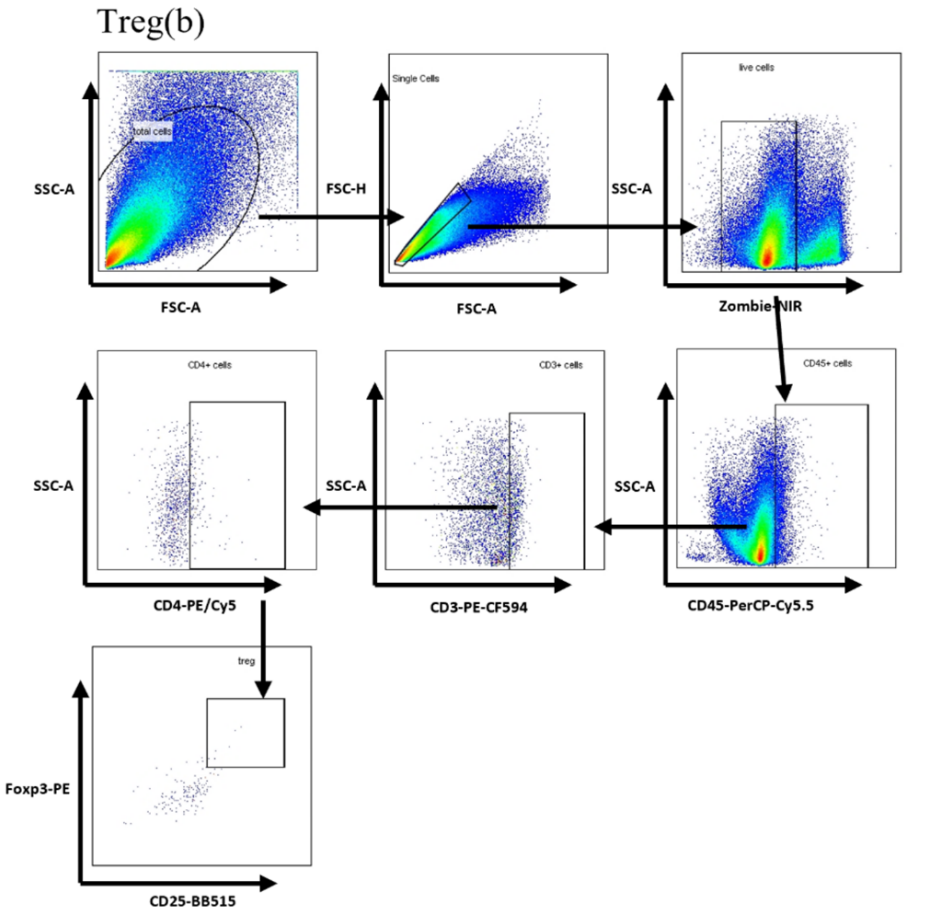
Treg(b)
total cells
SSC-A
FSC-A
Single Cells
FSC-H
FSC-A
live cells
SSC-A
Zombie-NIR
CD4+ cells
SSC-A
CD4-PE/Cy5
CD3+ cells
SSC-A
CD3-PE-CF594
CD45+ cells
SSC-A
CD45-PerCP-Cy5.5
treg
Foxp3-PE
CD25-BB515

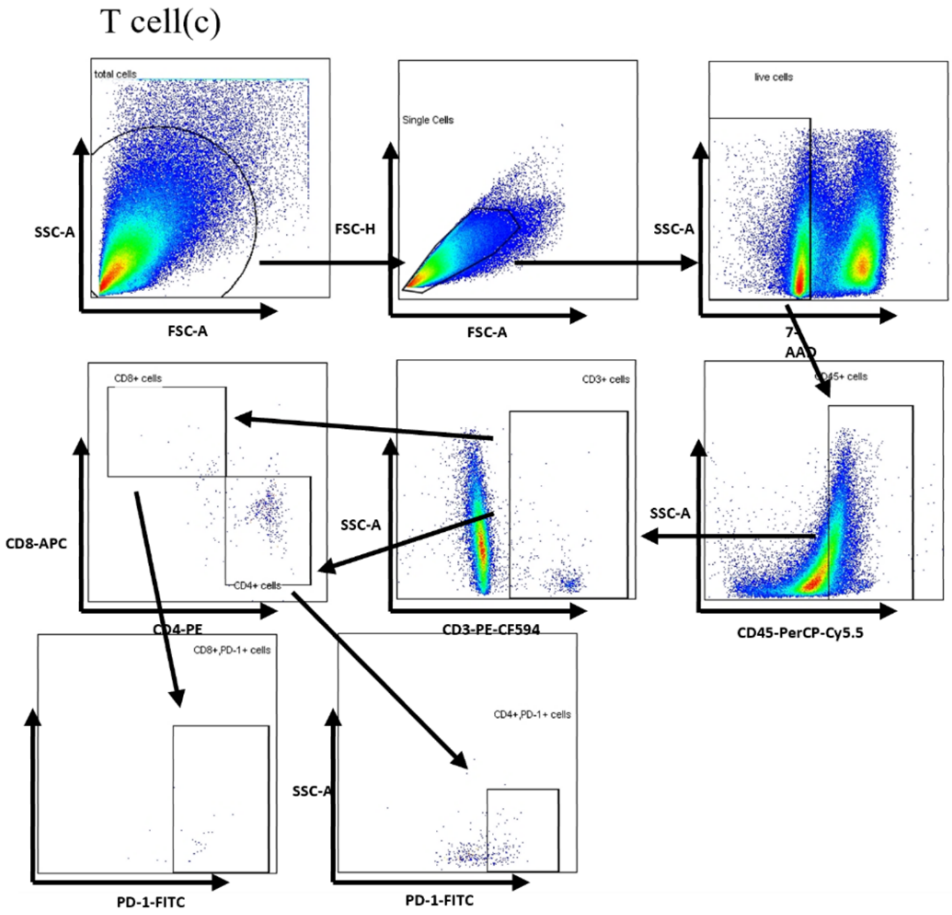
T cell(c)
total cells
SSC-A
FSC-A
Single Cells
FSC-H
FSC-A
live cells
SSC-A
7-AAD
CD8+ cells
CD8-APC
CD4+ cells
CD4-PE
CD3+ cells
SSC-A
CD3-PE-CF594
CD45+ cells
SSC-A
CD45-PerCP-Cy5.5
CD8+,PD-1+ cells
PD-1-FITC
CD4+,PD-1+ cells
SSC-A
PD-1-FITC

Supplementary Figure 4. A. Tumors of A2780 cells xenograft treated with PPS, DDP, or AE-848 (20 or 40 mg/kg/2 days intraperitoneally) for 2 weeks. The ruler scale is in centimeters. B. Growth curves of tumors in nude mice treated with PBS, DDP, or AE-848. C. Comparison of the weight of tumors in three treatment groups of nude mice. D. The expression of IGF2BP3and Ki-67 in tumors detected by IHC. E. The fractions of tumoral Treg cells, $CD4^+$ and $CD8^+$ T cells. F. Flow cytometry circle gate protocol.